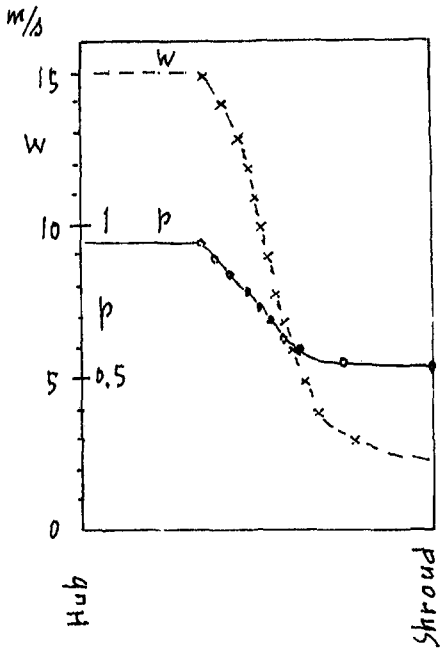

Fig. 22 Profiles of the throughflow w and the dimensionless rotary stagnation pressure p across the longitudinal vortex low for the direction from hub to shroud in the outlet section of the impeller

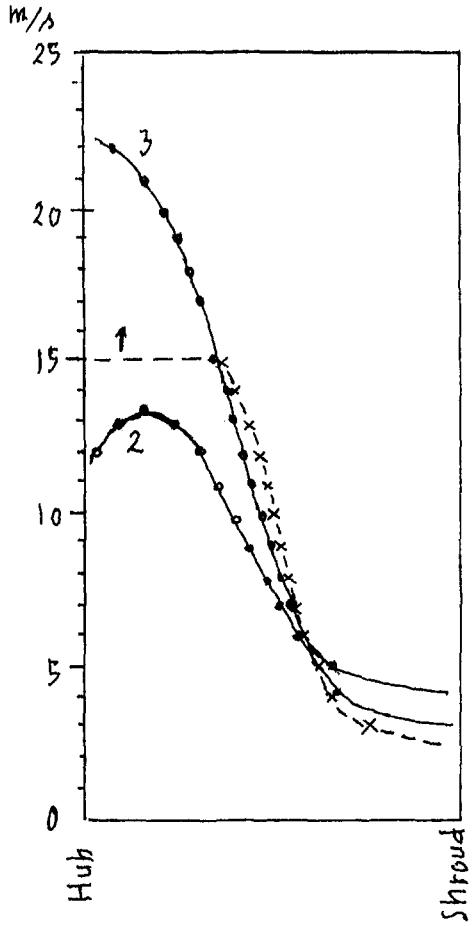

Fig. 24 Comparison of the profiles of the throughflow velocities w between the impeller outlet (curve 1 for normal operating point) and the diffuser inlet (curve 2 for low off-design flow at 84 percent and curve 3 for high off-design flow at 111 percent)

Y. N. Chen[2]

The authors have continued their very interesting series about secondary flows in centrifugal compressors.

If a comparison is made between the secondary velocity field at the inlet of the vaneless diffuser displayed in Fig. 21(c, d) (taken over from Figs. 3 and 4 of the paper) for the load of slightly above and below the design point on one hand, and the relative secondary velocity field at the outlet of the impeller for the normal operating point given in Fig. 21(b) (taken over from a previous paper of the series carried out by Farge and Johnson, 1990) on the other hand, a quite striking difference can be discovered, despite the very small gap of $0.02R_o$ between the impeller outlet and the diffuser inlet quoted. The relative secondary velocity field over the passage wake in the outlet of the impeller (Fig. 21(b)) shows a clockwise rotational direction, accompanied by a component pointing from hub toward shroud. But the secondary velocity field for the inlet of the diffuser (Fig. 21(c, d)) shows an anticlockwise rotational direction, accompanied by a component pointing from shroud toward hub. The two sets of the flow fields are completely reversed in the direction against each other. The secondary velocity field in Fig. 21(b) cannot be directly transferred into that in Fig. 21(c) or 21(d) by a linear transformation from the rotating frame of the impeller to the absolute frame of the diffuser. The reason for this intransferability must lie in the nonpotential behavior of a certain component of the flow system considered. This component is the passage wake in the blade channel of the impeller.

As shown in the paper of Chen et al. (1991), the passage wake in the blade channel of the impeller is enveloped by a longitudinal vortex, which rotates in the same sense as the projection on this vortex axis of the rotation vector of the impeller axis. This longitudinal vortex is therefore termed "vortex low L" according to the meteorological terminology. It is this vortex that isolates the passage wake of the low velocity against the surroundings of the high velocity.

The velocity field around the center of the passage wake in Fig. 21(b) clearly reveals the rotation pattern of its core, which lies in the deep pressure center depicted in Fig. 21(a). The profiles of the pressure p and the throughflow w across the core of this vortex low for the direction from hub to shroud are evaluated from Fig. 21(a, b) and plotted in Fig. 22. The two

[2] Sulzer Brothers Ltd., Winterthur, Switzerland.

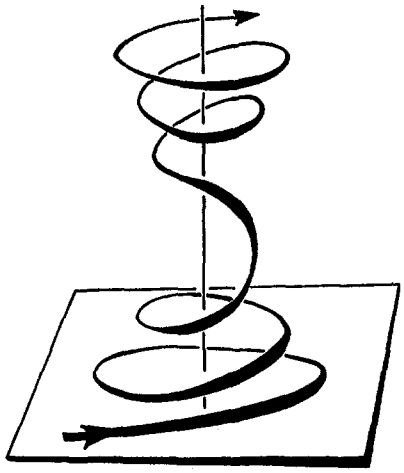

Fig. 23 Conversion of the cyclonic flow of the eyewall of the hurricane into anticyclonic flow when rising out of the eye into the upper free atmosphere (Lugt, 1983)

profiles coincide well with each other with respect to the vortex property of the secondary flow.

The deficit in the velocity along the core of the vortex originates from the secondary axial flow through the core within the mean flow field of the surroundings. Therefore, the gradient of the throughflow velocity field around the vortex core is very steep; see $w = 12$ to 5 m/s in Fig. 22. A concentrated secondary flow travels through the core of the vortex backward into the impeller.

The longitudinal vortex low of the blade channel of the impeller is formed along the shroud surface. Since, at the same time, this surface is perpendicular to the rotating axis of the impeller, it also behaves as the surface of a rotating disk. Then, the longitudinal vortex low L is embedded in the Ekman layer of this disk. Therefore, additional Ekman layer vorticity reinforces its intensity.

When this longitudinal vortex has left the impeller as a rotating system, and travels into the diffuser as an absolute frame, the feeding of the vorticity to the vortex ceases to take place. The vortex will expand, similar to the process of vortex compression occurring in the upper region over the eye of a hurricane (Whipple, 1983).

The high-speed rotation of the eyewall is caused by the spirally inward movement of the wind along the Ekman layer of the ground. Due to conservation of the angular momentum, the cyclonic motion of the wind is accelerated to a very high value when reaching the eyewall. During the acceleration, the vorticity of the spirally moving wind increases up to the region of the eyewall, in which the vorticity becomes maximum.

The wind then bends upward into the eyewall and rotates rapidly with it. When the wind has come out of the eyewall into the upper free atmosphere, the feeding of the vorticity no longer exists. The vortex formed by the wind then suffers from the compression with the result of expanding outward. The vorticity of the wind decreases rapidly to its negative value. Then, the rotational movement of the wind reverses its sense and becomes anticyclonic. This is shown in Fig. 23 (Lugt, 1983).

The development of the longitudinal vortex low L coming out of the rotating impeller to the absolute frame of the diffuser will undergo the same process as described above for the wind coming out of the eye of the hurricane. The vortex will expand (Fig. 24) and reverse its rotational sense to the opposite direction. It then becomes a vortex high H with the fluid coming out of the vortex.

The experimental series under the present discussion reveals a valuable phenomenon that the secondary longitudinal vortex low L of the rotating impeller is transferred to the secondary vortex high H, when it travels into the vaneless diffuser as an absolute frame. The vortex compression forms the fundamental mechanism in this transformation process. This process, which is familiar for the hurricane, in thus found in the turbomachinery.

References

Chen, Y. N., Seidel, U., Haupt, U., and Rautenberg, M., 1991, "The Rossby Waves of Rotating Stall in Impellers, Part II: Application of the Rossby-Wave Theory to Rotating Stall," *1991 Yokohama International Gas Turbine Congress, Proceedings,* pp. I/77–88.

Lugt, H. J., 1983, *Vortex Flow in Nature and Technology,* Wiley, New York, pp. 152–153.

Whipple, A. B. C., 1983, *Der Planet Erde, Stürme,* Time-Life Bücher, Amsterdam, pp. 84–90.

Authors' Closure

Response to Prof. N. A. Cumpsty's Discussion. The strong axial component of velocity near the hub wall observed at the above design flow rate in Figs. 3, 5, 7, 9, 11, and 13 is quite distinct from the much weaker component observed for the below design flow rate. This difference also led the authors to question the accuracy of the design flow rate results. For this reason the measurements at station 1 were repeated using different hot-wire probes and a fresh calibration. The velocity results obtained were to within ± 1 m/s in magnitude and ± 5 deg in direction to those shown in Fig. 3, which suggested that the results were repeatable and that the instrumentation had been correctly calibrated. A further check was made by examining the raw data (anemometer voltages and effective cooling velocities) from the double wire (Dantec 55P61). This was arranged with the two wires in the axial–radial plane, with each wire at 45 deg to both the radial and axial directions. Thus, in the case where the axial velocity component is very small, the effective cooling velocity will be the same for both wires. Conversely, if a large axial component exists, the two effective cooling velocities will be significantly different. In the below design case near the hub the two effective cooling velocities were very similar, whereas in the above design case very different values were obtained, which is consistent with the results in Figs. 3 and 4. The authors therefore believe the high axial velocities depicted near the hub at the above design flow rate to be correct.

The most likely explanation for these axial velocities would seem to be diffusion of the flow near the hub wall as the boundary layer thickens. If the maximum radial velocity contour values are considered for stations 1, 2, 3, 4, 6, and 8, these are 12, 12, 11, 11, 12, and 12 m/s at the below design flow rate and 22, 20, 19, 16, 17, 16 m/s at the above design flow rate. This suggests negligible diffusion for the below design flow rate, but strong diffusion from stations 1–4 at the higher flow rate. Furthermore, the peak radial velocity is very close to the hub at the above design flow rate, whereas the hub boundary layer has already thickened at station 1 and the peak is observed at $z/z_0 \simeq 0.2$ for the lower flow rate.

Response to Dr. Y. N. Chen's Discussion. The authors thank Dr. Chen for a very interesting explanation for the change in direction of vorticity within the passage wake as it travels from the last impeller station to the first diffuser station. An alternative explanation relates to the shroud wall boundary condition. The impeller is a shrouded impeller and hence in the wake close to the hub the relative tangential velocity is zero and hence absolute velocity is wr in PS to SS direction (left to right in Fig. 21*b*) as the flow leaves the impeller. When the flow enters the diffuser, this absolute tangential velocity is reduced to zero on the diffuser wall, which leads to very high levels of anticlockwise vorticity close to the shroud. This vorticity will diffuse away from the wall with distance downstream. The rate of diffusion will be high (with distance downstream) in the passage wake as the radial velocities in the wake are very low (less than 5 m/s) and hence the anticlockwise vorticity will quickly overcome the weak clockwise rotation observed in the passage wake in the impeller in Fig. 21(*b*).